Performance comparison of optical interference cancellation system architectures

Maddie Lu,[1,*] Matt Chang,[1] Yanhua Deng,[2] and Paul R. Prucnal[1]

[1]Department of Electrical Engineering, Princeton University, Princeton, New Jersey 08544, USA

[2]Bascom-Hunter Technologies, 341, 3rd Street, Baton Rouge, Louisiana 70801, USA

*Corresponding author: madelilu@princeton.edu

Received 11 January 2013; revised 6 March 2013; accepted 6 March 2013;
posted 7 March 2013 (Doc. ID 183169); published 10 April 2013

The performance of three optics-based interference cancellation systems are compared and contrasted with each other, and with traditional electronic techniques for interference cancellation. The comparison is based on a set of common performance metrics that we have developed for this purpose. It is shown that thorough evaluation of our optical approaches takes into account the traditional notions of depth of cancellation and dynamic range, along with notions of link loss and uniformity of cancellation. Our evaluation shows that our use of optical components affords performance that surpasses traditional electronic approaches, and that the optimal choice for an optical interference canceller requires taking into account the performance metrics discussed in this paper. © 2013 Optical Society of America

OCIS codes: (060.2360) Fiber optics links and subsystems; (060.4510) Optical communications; (060.5625) Radio frequency photonics.

http://dx.doi.org/10.1364/AO.52.002484

1. Introduction

Cosite interference is a widely known problem in communications, in which the presence of a closely located strong transmitter interferes with a radio receiver's ability to operate properly. Many solutions, ranging from traditional electronics to optical signal processing, have been proposed since the 1980s to mitigate the issues of cosite interference. Optical signal processing is a relatively new approach toward interference cancellation and a promising alternative to the bandwidth-limited electronics-based approaches. Bandwidth limitations are among the downfalls of electronics-based approaches, along with vulnerability to electromagnetic interference (EMI) and limited depth of cancellation due to precision-limited components [1,2]. The plethora of traditional interference cancellation approaches is too lengthy to discuss in full detail, but a variety of electronic (analog and digital) interference cancellation techniques will be reviewed. A review of traditional electronics-based approaches to interference cancellation makes clear the limitations of historical approaches and where optics can offer a better alternative.

The optical approaches evaluated in this paper stem from the earlier work of Suarez *et al.* [2], Bruno [3], and Suarez and Prucnal [4,5]. In short, these optical interference cancellation approaches involve combining the corrupted received signal with a sample of the transmitted (interfering) signal, which is optically weighted, delayed, and inverted such that it destructively interferes with the cosite interference contained in the received signal. The magnitude and delay adjustments mimic the transformations that the transmitted signal experiences as it propagates through a communication channel (i.e., over-the-air channel distortions).

Although the general idea behind optical interference cancellation remains the same, the actual implementations of an optical interference cancellation system can vary widely. In this paper, we propose

1559-128X/13/112484-10$15.00/0

various incoherent (use of two distinct optical wavelengths for modulating the received and transmitted signal), coherent (use of a single optical wavelength for electro-optic modulation), and direct modulation architectures for implementing an opto-cancellation system (OCS). The implementation details for the individual architectures will be discussed in Section 4.

The purpose of this paper is to develop a set of performance metrics upon which all optical interference cancellation architectures can be evaluated, and to analyze the incoherent, coherent, and direction modulation approaches against this set of metrics. Section 2 provides a background for the interference cancellation problem and describes the traditional efforts that have been put forth and the performance they have achieved. Section 3 describes the basis for comparison that will be used to evaluate the various optical interference cancellation architectures. Section 4 describes/demonstrates the details of the various architectures. Section 5 compares the performance of the various architectures based on the metrics described in Section 3.

2. Background

A. Interference Cancellers

The techniques and architectures to be presented were developed in an effort to combat the issue of cosite interference. Here, cosite interference corresponds to the situation where a receiver is located in close proximity to a strong transmitter, and extracting or detecting a weak signal from the receiver is extremely difficult, if not impossible. Since the 1980s, electronics-based solutions have been discussed and proposed, but these techniques were inherently limited by susceptibility to EMI, inability to combat in-band interference, and operational bandwidth concerns [1,2,5–7]. An optical approach to interference cancellation alleviates the need for this concern, since our optical approaches are fiber based and inherently immune to EMI. In addition, optical components do not have restrictions in terms of operating frequencies and are thus considered bandwidth insensitive. The advantages/disadvantages of traditional and optical approaches will be elaborated upon in the following sections.

B. Traditional Analog Approaches

Existing electrical-based interference cancellation systems can be divided into two main categories: analog and digital. Analog approaches to interference cancellation operate directly on the received and interfering signal, whereas digital approaches require sampling and digitizing of the signals.

One of the most commonly encountered analog interference cancellers is the Quellan QHx220 chip; this chip is commonly used in a variety of handsets to counter cosite interference between numerous antennas contained within the handset. In cell phones, this chip is used for combating EMI and boosting quality in areas with weak signal strength; it does so by canceling out interference from nearby antennas on the headset along with noise from the processor, camera, and display [8]. The interference cancellation is performed by an active signal-processing circuit that samples the noise source and emulates the RF coupling channel between the receiving and transmitting antennas. This emulation is then used to generate a cancellation signal. It uses the in-phase and quadrature control voltages to adjust the magnitude and phase of the cancellation signal. This cancellation signal is applied directly at the receive antenna to effectively undo the interfering effects of noise sources in the area surrounding the antenna. The QHx220 is capable of achieving 20–25 dB cancellation over a 10 MHz bandwidth, but its limitations include input signal power constraints as well as being constrained to operating on a finite number of modulation formats.

A group from Stanford university is working on another analog interference canceller. Their interference canceller is being developed for the purpose of mitigating cosite interference to enable full duplex communications. Communicating nodes must be able to simultaneously transmit and receive in order to facilitate full duplex communications; the limiting factor to full duplex communications is that nodes currently "hear" their own transmissions, along with the desired signal of interest. The proposed full duplex system setup includes a cancellation architecture that obtains a "perfect" inversion of the interfering signal and sums this inverted interferer with the received signal to extract only the desired signal of interest [9]. It is important to note that "perfect" inversion is achieved in an unconventional way; instead of using phase adjustments to achieve signal inversion, the proposed duplex system utilizes a balanced/unbalanced (balun) transformer to invert the interferer. The primary advantage to using a balun is that it eliminates the bandwidth constraint of the canceller; phase adjustments are inherently bandwidth limited, whereas a balun transformer is capable of simultaneously inverting all of the frequency components of a given signal. After the balun transformer inverts the interfering signal, the remainder of the cancellation scheme is like most others, where the inverted signal is then amplitude and phase adjusted to match the effects of the communication channel. This balun cancellation circuit has experimentally demonstrated 45 dB of cancellation over a 40 MHz wide signal [9]. The limitations to this balun-based approach include the inability to combat multipath components in a node's self-interference, which leads to an inability to perfectly emulate over-the-air losses encountered in the communication channel.

C. Traditional Digital Approaches

Wireless communications depend strongly on interference cancellation schemes, and the predominant approach used includes a number of digital signal processing techniques. With digital-signal-processing based approaches, the signal is sampled via an

analog-to-digital conversion before it is operated upon. Once the interference cancellation is complete, the processed signal is usually then converted back to an analog version and passed to the receiver system.

Perhaps the most commonly encountered digital interference mitigation technique is the use of the matched filter. A matched filter approach is used for channel estimation and compensation; a pilot signal is transmitted to generate an impulse response of the channel, and this impulse response is then used to generate a matched filter, which creates an inverse of the channel response. The matched filter is constructed via a series of tapped weights and delays that attempt to generate the inverse of the communication channel's impulse response characteristic. This transversal filter approach is widely used in canceling clutter and multipath reflections in passive radar [10], and the topic of adaptive transversal filtering is discussed at length in [11]. Matched filtering has been able to achieve approximately 30 dB of cancellation over a 10 MHz bandwidth and is primarily plagued with bandwidth constraints; these arise from the inherent bandwidth limitation of electronic components as well as the bandwidth constraint imposed by the dynamic range of analog-to-digital converters.

Related to matched filtering is the concept of Rake receivers, which are commonly used today to combat multipath effects in wireless radio, particularly code-division multiple access. A Rake receiver is composed of several subreceivers, called "fingers", each of which is dedicated to decoding an individual multipath component. To do so, each finger applies an appropriate weight and delay that mimics the amplitude and delay adjustments encountered when the signal travels a path other than the line-of-sight path. Assuming that the receiver is able to accurately account for the amplitude and delay adjustments for each multipath component, the signal quality and reliability at the receiver end should greatly improve [12]. The challenge with Rake receivers is that they require good knowledge of the channel in order to discretize the multipath components. Incorrectly placed fingers can worsen performance, and finger placement is an optimization problem that requires balancing system performance and complexity, because constant iterations of channel estimation/compensation through finger placement are computationally costly [13–15]. Rake receivers are common and effective in the wireless industry, but there is a great amount of research focused on improving the complexity and efficiency of these digital interference cancellers.

D. Optics-Based Interference Cancellers

Discussion of an optics-based interference canceller can be traced back to the work done at MIT Lincoln laboratory in the early 1990s [16,17]. The researchers were most concerned with proposing an electro-optic interference canceller to address the inadequate channel-tracking capabilities of electronic interference cancellers. Electro-optic modulators showed promise, because once the RF signal is optically modulated, it then occupies only a small fractional bandwidth, allowing for close channel tracking [16]. The proposed nulling system included switchable optical delay lines to compensate for dispersion, along with a series of controllable complex optical weights to allow for amplitude and phase adjustments.

In 2007, Boeing filed a patent for an interference rejection system that included an optical subsystem. Similar to standard cosite interference rejection systems, the patented canceller includes a coupled connection to the transmit system, and the interference rejection subsystem operates on a sampled copy of the transmit system. The interference subsystem weights the sampled transmit signal, such that the weighted signal cancels destructively with the interfering component in the received signal. The unique aspect to Boeing's proposed system is the optical subsystem, in which the signal from the receive antenna is combined with the weighted signal from the interference subsystem and used to drive the optical subsystem [18]. The desired receive signal is derived by converting the output of the optical subsystem to an electrical signal. The benefits provided by the use of an optical subsystem address the limitations posed by electronic interference cancellation systems. Namely, the signals cancel in the optical domain, which means that they avoid the nonlinearity issues of dealing with electrical components, and the optical subsystem is capable of handling and operating on the high power interferer signals, which would otherwise saturate low-noise amplifiers used in electronic interference cancellation systems. Improved architectures for optical interference cancellers will be presented in detail in Section 4.

3. Basis for Comparison

As mentioned previously, a standard basis for comparison must be developed upon which we can evaluate current and future system architectures for achieving optical interference cancellation. The performance parameters against which we have decided to evaluate the various cancellation architectures include standard measures of performance for RF photonic links, along with notions of operational wavelength, cancellation bandwidth, and depth of cancellation.

A. Link Loss

Link loss describes the loss incurred when a signal traverses the link in question, and encompasses the loss caused by couplers, adapters, passive components, and electro-optic conversions. Link loss is a significant system measure because lossier systems will usually necessitate the use of an amplifier at some point in the link, but amplifiers introduce their own problems, which include but are not limited to insertion loss, nonlinearity, and noise amplification. Depending on the requirements posed by the specific application of interference cancellation, some amount of these limiting factors may be tolerable, and the scenario in question dictates the use of amplification to improve link loss:

$$\text{Loss}_{\text{link}} = P_{\text{output,electrical}} - P_{\text{input,electrical}}. \quad (1)$$

Link loss is related to the physical phenomenon of electrical-to-optical conversion; the larger portion of the link loss occurs at the interface between the electrical and optical signals. At the modulator, imperfect coupling between the electrical RF signal and the optical signal in the waveguide can lead to an inefficient electrical-to-optical conversion. Electrical leakage to the modulator substrate can be caused by phase mismatch between the waveguide and substrate modes in the modulator, which then creates coupling loss [19]. At the optical-to-electrical conversion in the photodetector, link loss could be improved with increased optical power into the photodetector, but the problem here is that high-speed photodetectors feature small active areas, resulting in lower power saturation thresholds [20].

B. Dynamic Range and Linearity

Dynamic range is a measure of the power range of a system and reflects the difference between the minimum and maximum signal strengths of a given system. Unlike link loss, dynamic range is less of an inherent characteristic of a given system and is more of a design parameter when building and implementing an interference canceller. The dynamic range required in an interference canceller depends on the strength of both the signal of interest and the interferer, and the dynamic range could vary greatly across a spectrum of various cosite interference scenarios.

Specifically, we use the notion of spur-free dynamic range (SFDR) in our measurements of the performance of our optical interference cancellation system. SFDR refers to the difference between the minimum detectable signal and the maximum signal that can be introduced into the system without distortion [21]. At the same time, SFDR measurements give a good indication to the overall linearity of a given system. The purpose of these measurements is to determine at which input signal power levels the system begins to display nonlinear behavior, generating nontrivial mixing effects and harmonics.

To briefly summarize the SFDR measurement procedure, two tones of different frequency but equal signal power are input to the link under test, and the output signal is analyzed on an RF spectrum analyzer. As the power of the input signals is varied, the strengths of the harmonics and intermodulation products relative to the carrier tones also change, and as the input power increases, the harmonics and mixing products become more profound and give indication as to the linearity and dynamic range of the link under test. Intermodulation products indicate the mixing that occurs when signals of two or more frequencies generate output signals at sum and difference frequencies (i.e., not just the harmonic multiples of the individual frequencies). The artifacts at the sum and difference frequencies are indicative of the nonlinearity of the system, as a linear system would only output the original (fundamental) signal.

The signal strengths of the output signals (both the fundamental and the harmonics and intermodulation products) are plotted against the strength of the input signal. The trends are then linearly fit, which results in a gain slope of approximately 1 for the fundamental trend and a gain slope of approximately 3 for the third-order intermodulation products.

The linear fit trendlines are used to calculate an important data point, the third-order input intercept point (IIP3). The IIP3 refers to the input power level at which the fundamental and third-order intermodulation trendlines intercept, and represents the point at which the third-order intermodulation products overpower the fundamental signal. It is important to note that the IIP3 is not a measurable quantity; it is strictly a calculated figure, as it usually surpasses the damage threshold of the device or system under test.

In order to calculate the SFDR, the noise figure (NF) is required, and can be calculated or measured in a number of ways [22]. The NF reflects a specific device or system's contribution to noise in a specified link; in other words, it quantifies the degradation in signal-to-noise ratio over a specific link. For our calculations and comparisons, we use the calculation-based gain method for determining the NF based on the output noise power, system bandwidth, and system gain, along with the standard background thermal noise (BNL) of −174 dBm/Hz. With the following equation, we are able to determine the NF of various OCSs:

$$\text{NF} = P_{\text{noise,out}} - (-174\ \text{dBm/Hz} + 10\log_{10}(\text{BW}) + \text{Gain}). \quad (2)$$

The equation below is used to express the SFDR in terms of the IIP3, the BNL of −174 dBm/Hz, the system bandwidth (BW), and the NF [21]:

$$\text{SFDR} = \frac{2}{3}(\text{IIP3} - \text{BNL} - 10\log_{10}(\text{BW}) - \text{NF}). \quad (3)$$

C. Optical Performance Parameters

Operational wavelength, depth of cancellation, and cancellation bandwidth are all performance parameters that are not standard measures of an RF photonic link. Instead, these parameters are specific to our development of an optical interference canceller.

Operational wavelength reflects the wavelength of the light source used in a given optical interference canceller and is usually expressed in units of nanometers (nm). Depending on the specific architecture and system implementation, there may be one or numerous operational wavelengths; coherent systems utilize a single light source, whereas incoherent systems utilize two or more light sources of distinct wavelengths.

Depth of cancellation is a straightforward measure of the performance of any interference canceller, regardless of whether it is optical or electrical. It is measured in units of decibels and reflects the

reduction in power of the interferer provided by the interference canceller. While it is easy to get distracted by large cancellation depths, it is important to also evaluate cancellation bandwidth, which is the trade-off often associated with depth of cancellation.

Cancellation bandwidth is a trade-off to depth of cancellation, because a large cancellation depth is usually indicative of narrowband cancellation, or cancellation of a small signal bandwidth. This depth versus bandwidth cancellation is due to the inherent trade-off associated with the time delay adjustment utilized in interference cancellation. As mentioned previously in Section 2, most (if not all) interference cancellation schemes involve modifying the weights and delays of a sampled interferer in such a way that the modified signal destructively interferes with itself. In order to achieve the signal delay modification, a variable delay line or phase shifter must be used, and inherent to these devices is a trade-off in granularity. Variable delay devices either have a broad tuning range and limited adjustment precision, or they have a very small tuning range with very fine adjustment precision. As a result, it is difficult to precisely match the actual delay necessary to create destructive interference. In addition, it is difficult to achieve deep cancellation over broad bandwidths because of a dispersive effect. Signals at different frequencies will experience different amounts of delay, and as a result, no single delay adjustment will compensate for the aggregate delay effects at various frequencies. Combined with the granularity trade-off of variable delay devices, depth of cancellation is limited by the shortcomings of the delay adjustment process in interference cancellation.

4. Architecture Details

The architectural details of the various optical interference cancellation systems will be discussed in this section.

A. Incoherent OCS

The incoherent OCS is named as such because of "incoherence" between the two arms of the cancellation system. Each arm's light source is of a distinct wavelength, and this incoherence allows for the circumvention of beating effects when the signals from both arms are combined. In our experimental incoherent system architecture, we utilize two "transmitter" modules from Linear Photonics, which include a self-contained distributed feedback laser and a Mach–Zehnder modulator. The two modulators are biased opposite one another, with one biased on the positive-slope linear region of the transmittance curve and the other biased on the negative-slope linear region; this allows us to achieve the signal inversion without using a phase shifting device. Delay adjustments are achieved using a micrometer-style variable optical delay line, which can provide up to 83 ps of variable delay. Attenuation adjustments are achieved using a microelectromechanical-systems-based variable optical attenuator, which is controlled by a Keithley 2400 SourceMeter that can provide adjustments on the order of .01 mA. After both arms are combined in a 50:50 2×2 optical coupler (one output channel is unused), a Linear Photonics "receiver" module containing a wide-bandwidth photodetector is used to convert the processed optical signal back to an electrical signal. The Linear photonics photodetector used in this incoherent architecture is different from the Discovery photodetector used in both the coherent and direct modulation architectures, because the modulator used in the incoherent setup was designed and sold as a "matched" modulator–photodetector pair. Similar attributes between the two photodetectors still make for valid comparison between the three architectures: both photodetectors operate from DC to 20 GHz, are capable of handling optical input $> +8$ dBm, and have a responsivity of ~0.8 A/W in the 1550 nm region.

An architectural diagram detailing the components of both the "received signal" arm and the "reference signal" arm are featured in Fig. 1.

B. Coherent OCS

Whereas the incoherent OCS utilizes two distinct light sources to avoid beating effects, a coherent architecture has been realized that utilizes a single light source while at the same time avoiding any

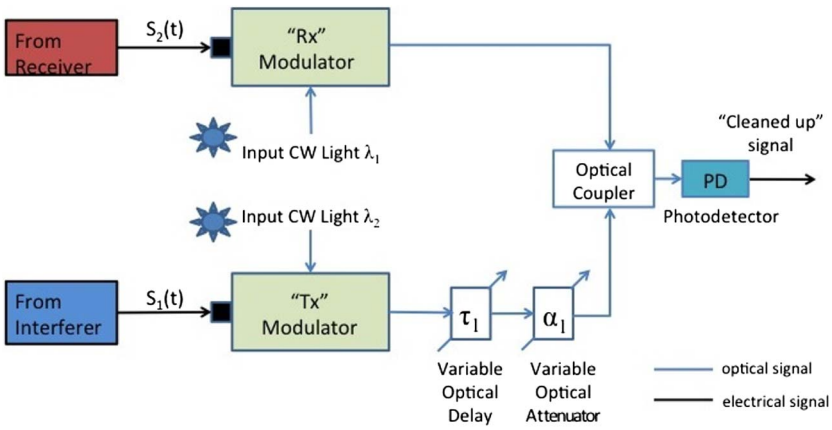

Fig. 1. System architecture for the incoherent OCS. Rx = received signal arm; Tx = reference/transmitted signal arm.

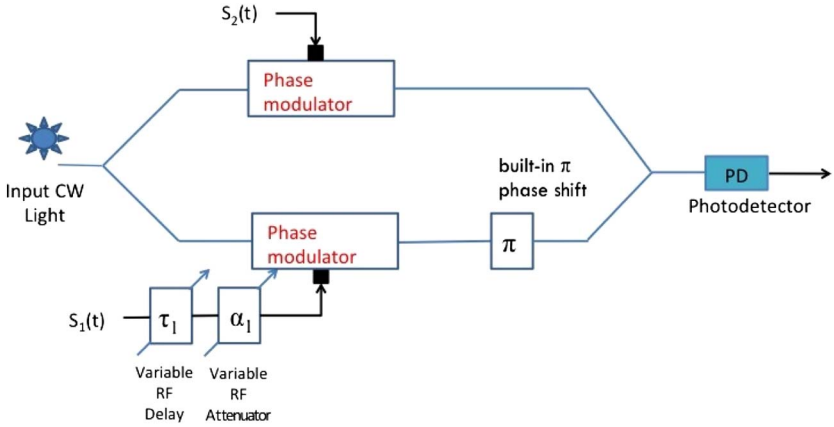

Fig. 2. System architecture for the coherent OCS.

beating effects. The unique feature of the coherent architecture is the use of a dual-drive Mach–Zehnder (DDMZ) modulator. The modulator has two arms, where each arm functions as a phase modulator and one of the arms includes a built-in π phase shifter. Each arm has its own input electrode for the driving RF signal, and similar to the setup of the incoherent OCS, one arm is driven by the received signal while the other arm is driven by a sample of transmitted/interfering signal. Instead of using variable optical delay and attenuation devices, the coherent OCS architecture varies the delay and attenuation in the RF domain. This predistortion technique modifies the signal before it is electro-optically modulated, which can prove to be a trade-off. The trade-off associated with using a DDMZ is that the signal distortion must be done electrically, which is a disadvantage because of the limited bandwidth and coarse granularity of electrical delay adjustments, as discussed previously in Section 2. To be specific, we consider the RF delay device as the source of our bandwidth limitations. The trombone-style RF delay lines that we used were limited in terms of operating frequency, as the listed range varied from 0.25 to 4 GHz, but their main limitation was in the range of phase/delay adjustments. The length of the slider affects frequency in that for a given length, there is an optimal lower limit for which the advertised phase/delay shift range applies. While the listed operating frequency range still applies for the device as a whole, signal frequencies below the lower limit as "defined" by the length of the shift would have a less-than-ideal range of phase/delay shift adjustments.

The benefit provided by the use of a DDMZ is that the device allows for complete cancellation of the interfering signal, because the signals from both arms of the DDMZ completely interfere destructively with one another at the output junction of the modulator; this is an advantage over the incoherent setup, where the use of two distinct wavelengths results in a DC level at the output even when the amplitude and delay adjustments are perfect. Our specific implementation utilized a JDSU-manufactured dual-electrode (drive) Mach–Zehnder modulator, along with a trombone-style RF line shifter and an RF attenuator to achieve the signal modification necessary. A wide-bandwidth Discovery photodetector was used to convert the optical signal back to an electrical signal, and an architectural diagram of the coherent OCS setup can be found in Fig. 2.

C. Direct Modulation

The final OCS architecture to be discussed is the direct modulation approach; here, the RF "driving" signal directly modulates the laser output. With this type of direct modulation approach, the need to rely on electro-optic modulators is avoided, which provides some additional benefits. The use of electro-optic devices allows for a much greater operational bandwidth compared to electrical-based interference cancellers, but electro-optic modulators still have some limitations. One of the performance-limiting factors of electro-optic-modulator-based OCSs is frequency response mismatch between the two arms of the system. This mismatch is more of an issue in the incoherent OCS, because it utilizes two off-the-shelf modulators that are not well matched, whereas the arms of the DDMZ in the coherent OCS are closely matched over a 10 GHz bandwidth. The frequency response mismatch affects depth of cancellation over broad bandwidths, because the difference in frequency response between two arms means that they will respond differently to the same input. With the direct modulation architecture, there is not such a glaring nonuniformity in the frequency response of the two arms of the system, as the system is limited only by the laser's modulating signal range. Similar to the incoherent architecture, the attenuation and delay adjustments are made in the optical domain, and the use of optical components avoids the frequency dependence that limits the coherent architecture. On the whole, the direct modulation architecture is rather simple; without the use of electro-optic modulators, the received and the sampled interferer signals are used to directly drive the lasers, and the inversion of the interferer is accomplished using an RF inverting amplifier. The optical attenuation and delay adjusting components are more or less the same as those used in

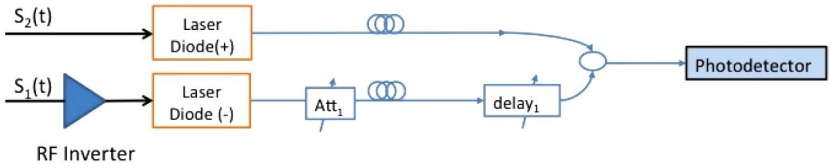

Fig. 3. System architecture for the direct modulation OCS.

the incoherent architecture, and a wide-bandwidth Discovery photodetector is still used to convert the optical signal back to its electrical counterpart. The direct modulation architectural diagram can be found in Fig. 3.

Table 1 summarizes the values and signal parameters used across the experiments and simulations for the three architectures.

5. Performance Comparison

In this section, we will evaluate the performance of the three OCS architectures based on the values and figures described in detail in Section 3. The conclusions of the performance comparisons below are based on experimental data as well as either simulations built in VPI Photonics Design and Simulation Suite or mathematical-based simulations performed in MATLAB.

A. Link Loss

In comparing the link loss of the three OCS architectures, there is similarity between both electro-optic modulation approaches but great variance between these electro-optic modulation architectures and the direct modulation approach. The incoherent and coherent architectures, which utilize electro-optic modulation, are inherently lossier than the direct modulation architecture due to the electrical–optical–electrical (E-O-E) conversion that occurs across the link. In the direct modulation approach, there is no electro-optic modulation or conversion, as the electrical signal directly modulates the laser, resulting in a smaller link loss. While the direct modulation approach appears to be substantially less lossy, there is some caveat to the link loss in Table 1. The photoreceiver used in the direct modulation approach has a built-in amplifier, which makes it impossible to separate the amplifier's gain contribution from the system's overall link loss.

Comparing the link loss of the incoherent and coherent architectures, the coherent approach is lossier than the incoherent approach, due to a combination of both electro-optic conversion losses (modulator and photodetector) in addition to the losses caused by the RF attenuator and delay line. In both the coherent and incoherent approaches, the modulator–photodetector combination is the source of the majority of the link loss. To improve the link loss figure, an amplifier could be used, but consideration must be taken with regard to the additional noise that the amplifier contributes, as well as the amplifier's additional limitations on the system's dynamic range and linearity.

B. Dynamic Range and Linearity

The dynamic range and linearity can be interpreted as a measure of the power tolerance of a given system; these quantities indicate the range of input powers for which the system behaves as it was designed. Again, the performances of the incoherent and coherent architectures were very different from the direct modulation architecture. Both the incoherent and coherent architectures had dynamic ranges >60 dB; the limiting factor to the dynamic range was the NF. Most notably in the case of the experimental data collected for the coherent architecture, the NF suffers simply because the link loss is so high. The noise floor and bandwidth were similar in all cases, but the experimentally measured link loss of the coherent system was −60 dB, compared to ∼− 30 dB for the incoherent architecture. A low-noise amplifier could be used to improve the link loss, but the trade-offs of using an amplifier need to be taken into consideration. Amplifiers add some amount of noise, they have a defined operational bandwidth (which is likely much smaller than that of the OCS), and they will introduce additional nonlinearities at higher gain settings.

The dynamic range of the direct modulation architecture was substantially better than that of the incoherent and coherent architectures. The link loss was much smaller for the direct modulation architecture, although part of the reason for the reduced link loss was the amplifier built into the photodetector used in the direct modulation architecture. While it is tempting to deem the direct modulation

Table 1. Summary of the Values and Signal Parameters Used in the Experiments and Simulations of the Direct Modulation, Incoherent, and Coherent OCS Architectures

Parameters	Direct Modulation	Experimental (Incoherent/Coherent)	Simulation (Incoherent/Coherent)
Wavelength	1330, 1550 nm	1550 nm	1550 nm
Optical input power	+6 dBm	+8 dBm	+8 dBm
RF signal frequency	500 MHz	1.5 GHz	1 GHz
Photodetector responsivity	0.7 A/W	0.8–1.0/0.8 A/W	1 A/W
Operational bandwidth	0.02–1 GHz	0.2–20 GHz	0–20 GHz
Maximum optical input power	+9 dBm	+10 dBm/+ 9 dBm	Not available
RF input signal power	0 dBm	0 dBm/+ 10 dBm	0 dBm/+ 10 dBm

architecture superior because of its low link loss and large dynamic range, there is another parameter to take into consideration: the IIP3. The direct modulation architecture has an IIP3 of 20 dBm, meaning that at an input power of 20 dBm, the third-order intermodulation products will dominate and overpower the fundamental signal. The IIP3 of the direct modulation architecture is noticeably lower than the IIP3 of the incoherent/coherent architectures, which means that the ideal operating input power range of the direct modulation architecture is much lower. While IIP3 and minimum detectable signal are two wholly separate and disparate parameters, one can easily imagine situations where the two parameters would be closely related. Strictly as an example, a system with a lower IIP3 might have a smaller minimum detectable signal, and for a given dynamic range, this would allow the system to operate on a wide range of low-power input signals.

It is important to note that dynamic range of a system is often dictated by the system's intended application, and comparison between two or more systems is not straightforward. As evidenced in the discussion of dynamic range, there are several other factors to take into consideration when evaluating a given system. The incoherent and coherent architectures have a smaller dynamic range, but given that their IIP3 is much higher than the direct modulation architecture, these architectures could prove to be better suited to an application geared toward processing larger-magnitude input signals. Again, thought must be given to a system's intended application when evaluating possible solutions.

Figure 4 summarizes, for the various architectures, the fundamental transfer function and intermodulation functions that were discussed in the prior section on dynamic range and linearity.

C. Optical Performance Parameters

The final piece to our performance comparison concerns the optical component to the various optocancellation architectures discussed throughout this paper. As discussed previously in Section 3, the optical performance parameters to be considered are operational wavelength, depth of cancellation, and operational bandwidth.

The operational wavelength of a given OCS is more of a distinction than a performance parameter. Optical sources are readily available in many wavelengths, and the wavelength mostly affects component compatibility; the laser source must be compatible with the modulator, which must be compatible with the photodetector. In the case of the incoherent setup, the optical wavelengths had to be chosen such that they both fell in the 1550 nm region but were separated enough to avoid coherent beating effects when the two arms of the channel are summed. The choice of wavelength in the coherent architecture was not critical, because the architecture only requires a single optical source, and the modulator used specified a wide range of input wavelengths in the 1550 nm region.

Depth of cancellation is a commonly used figure of merit in all cancellation systems, optical or not. In our discussion, we consider depth of cancellation for both narrowband interference as well as broadband interference. All three architectures perform narrowband cancellation extremely well, but there are some slight differences when it comes to canceling over large bandwidths. Take, for example, a bandwidth of 1 GHz. The incoherent and coherent architectures can achieve deep cancellation (>60 dB) over small, narrow bandwidths within this 1 GHz, while other regions within this 1 GHz bandwidth are only reduced by ~20 dB. Here, uniform cancellation over a large bandwidth is sacrificed for deep nulls at discrete frequencies. The direct modulation architecture

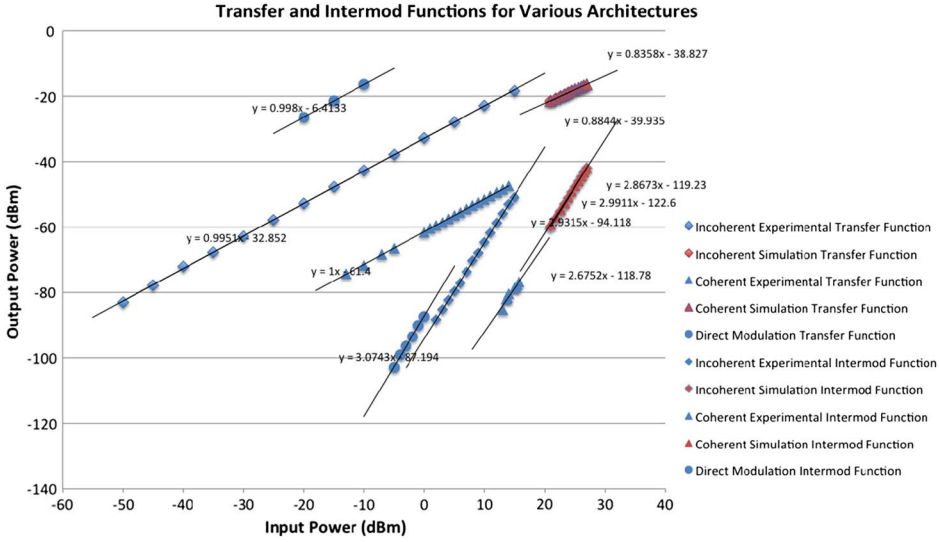

Fig. 4. Transfer functions and intermodulation functions for the incoherent, coherent, and direct modulation architectures. The linear-fitted trendlines indicate that the transfer functions have a slope of ~1 and that the intermodulation functions have a slope of ~3.

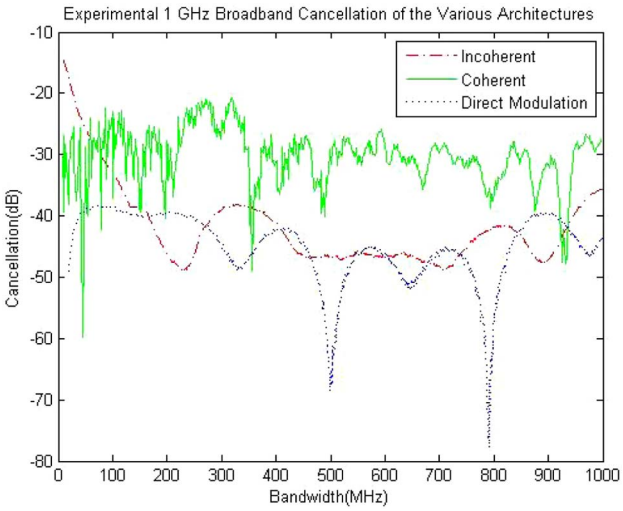

Fig. 5. Experimental depth of cancellation performance for broadband (1 GHz) cancellation for the incoherent, coherent, and direct modulation optical interference cancellation architectures.

behaves slightly better in terms of achieving decent cancellation depth without sacrificing uniformity, as it can achieve at least 40 dB of cancellation across a 1 GHz bandwidth, with some nulls reaching 75 dB of cancellation. Our preliminary thoughts regarding the better performance of the direct modulation architecture seem to point to the discrepancies between the electro-optic and direct modulation architectures with regard to frequency response. The incoherent and coherent architectures have a nonflat S21 frequency response, which correlates the modulated optical signal to the frequency of the input RF signal. Even though the S21 frequency response is relatively flat over the entire operating range of the modulators, there is still some fluctuation in the response characteristics that becomes evident when canceling over larger bandwidths, especially when considering large-bandwidth signals (greater than a few hundred megahertz). In the direct modulation architecture, the so-called "frequency response" is more a reflection of the impedance matching of the "premodulation" network, instead of the optical signal being dependent upon the frequency of the modulating RF signal. As we continue to experiment with canceling over large bandwidths, we are giving increased thought to evaluating architectures with flat frequency responses.

Figure 5 shows a depth of cancellation comparison across the incoherent, coherent, and direct modulation architectures for a broadband signal with 1 GHz of bandwidth.

As mentioned in the discussion on dynamic range, the intended application of a system is a significant factor in the evaluation of its performance. It is the same case when considering depth of cancellation, as characteristics of the interferer dictate the appropriate and necessary requirements for the cancellation system. For example, in the case of a low-power broadband interferer, an architecture that performs similarly to the direct modulation scheme would be better suited, as it is capable of uniform cancellation across a large bandwidth. If deep cancellation were more of a priority, then focusing on narrowband cancellation would likely be more advantageous in that scenario.

To summarize the performance metrics across the incoherent, coherent, and direct modulation architectures, Tables 2 and 3 feature the experimental and simulated measures of link loss, IIP3, dynamic range, NF, and depth of cancellation. We believe that the discrepancies between the experimental and simulation data arise due to the fact that the simulation software was limited in terms of how many parameters could be modified to reflect the experimental setup, which meant that we were not able to precisely mimic the experiments. The components used

Table 2. Summary of the Measured and Simulated Performance Parameters[a]

	Incoherent Experimental	Incoherent Simulation	Coherent Experimental	Coherent Simulation	Direct Modulation (with preamplification and postamplification)
Link loss	−32 dB	−42 dB	−61 dB	−42 dB	−5 dB
IIP3	34.3 dBm	33.3 dBm	31.9 dBm	33.6 dBm	20 dBm
NF	54 dB	69 dB	84 dB	73 dB	30 dB
SFDR	83 dBm/Hz$^{2/3}$	65 dBm/Hz$^{2/3}$	61 dBm/Hz$^{2/3}$	64 dBm/Hz$^{2/3}$	107 dBm/Hz$^{2/3}$

[a]Link loss reflects the overall system gain being negative, since it relates the output power to the input power, and without the use of an amplifier, the output power is always lower than the input power. The link loss of the direct modulation approach appears dramatically lower than the incoherent and coherent approaches because of the amplifier built into the photoreceiver.

Table 3. Summary of the Depth of Cancellation Experimentally Achieved by the Incoherent, Coherent, and Direct Modulation Architectures of the OCS for both Narrowband and Broadband Interferers

	Incoherent	Coherent	Direct Modulation
Narrowband cancellation	80 dB	60 dB	80 dB
Broadband cancellation	25 dB (min)	20 dB (min)	40 dB (min)
(1 GHz bandwidth)	70 dB (max)	60 dB (max)	75 dB (max)

in the simulation were the same devices as those used in the laboratory experiment, but some of the device-specific parameters in the simulation could not be tweaked to precisely match those used in the laboratory. As an example, the Mach–Zehnder modulator in the simulation had a greater modulation loss than the Linear Photonics XiMod unit used in the experiments, and the VPI simulation module could not be modified to reflect the behavior of the Linear Photonics modulator unit. That being said, we believe that we our simulations captured the fundamental essence of our experiments and served as a useful validity reference for our experimental results.

6. Conclusion

Over the course of this paper, we have highlighted some noteworthy accomplishments in the field of interference cancellation, setting the stage for a proper evaluation of innovative techniques toward combating the limits posed by electronic means of interference cancellation. The collection of performance parameters put forward is nowhere near conclusive and should merely serve to guide preliminary discussion and evaluation of future optical interference cancellation systems. Our performance evaluations have given us reason to delve further into the direct modulation architecture, and future work will include proper characterization of the system to better understand its performance.

The authors would like to thank Dr. M. Fok and J. Chang for their invaluable guidance and discussion. This work is supported by Princeton University STTR grant no. 339-6463 and SSP TCN 12043.

References

1. A. Seeds and K. Williams, "Microwave photonics," J. Lightwave Technol. **24**, 4628–4641 (2006).
2. J. Suarez, K. Kravtsov, and P. Prucnal, "Incoherent method of optical interference cancellation for radio-frequency communications," IEEE J. Quantum Electron. **45**, 402–408 (2009).
3. J. Bruno, "Electro-optic cosite interference mitigation," Proc. SPIE **7607**, 76071A (2010).
4. J. Suarez and P. Prucnal, "Characterization of the instantaneous bandwidth of counter-phase optical interference cancellation," IEEE Photon. Technol. Lett. (2009).
5. J. Suarez and P. Prucnal, "System-level performance and characterization of counter-phase optical interference cancellation," J. Lightwave Technol. **28**, 1821–1831 (2010).
6. F. J. Kub, E. W. Justh, and B. Lippard, "Self-calibrating hybrid analog CMOS co-site interference canceller," in *MILCOM Proceedings 1999* (IEEE, 1999), Vol. **2**, pp. 1051–1054.
7. F. J. Kub and E. W. Justh, "Analog CMOS implementation of high frequency least-mean-square error learning circuit," IEEE J. Solid-State Circuits **30**, 1391–1398 (1995).
8. Quellan QHx220 datasheet, http://www.anglia-m2m.com/GPS/intersil/QHx220.pdf.
9. M. Jain, J. I. Choi, T. M. Kim, D. Bharadia, S. Seth, K. Srinivasan, P. Levis, S. Katti, and P. Sinha, "Practical, real-time, full duplex wireless," in *IEEE MobiCom 2011* (ACM, Las Vegas, Nevada, 2011), pp. 301–312.
10. R. Cardinali, F. Colone, C. Ferretti, and P. Lombardo, "Comparison of clutter and multipath cancellation techniques for passive radar," in *2007 IEEE Conference on Radar* (IEEE, 2007), pp. 469–474.
11. B. Widrow and S. D. Stearns, *Adaptive Signal Processing* (Prentice-Hall, 1985).
12. http://www.smsmatrix.com/front/mob_doc/tech-1/chaptr05/cdma/rake.html.
13. G. Bottomley, T. Ottosson, and Y.-P. E. Wang, "A generalized RAKE receiver for interference suppression," IEEE J. Sel. Areas Commun. **18**, 1536–1545 (2000).
14. D. Cassioli, M. Z. Win, F. Vatalaro, and A. F. Molisch, "Low complexity rake receivers in ultra-wideband channels," IEEE Trans. Wireless Commun. **6**, 1265–1275 (2007).
15. N. Boubaker and K. B. Letaief, "A low complexity MMSE-RAKE receiver in a realistic UWB channel and in the presence of NBI," in *IEEE Wireless Communications and Networking* (IEEE, 2003), Vol. **1**, pp. 233–237.
16. A. Sonnenschein and W. K. Hutchinson, "A design for an electro-optic implementation of a wideband nulling system," in *MILCOM 1990* (IEEE, 1990), Vol. **2**, pp. 742–748.
17. L. M. Johnson, H. V. Roussell, and G. E. Betts, "Interferometric modulators for an adaptive nulling system," Proc. SPIE **1790**, 50–54 (1993).
18. M. J. LaGasse, "Cosite interference rejection system using an optical approach," U.S. patent 7,231,151 (12 June 2007).
19. G. K. Gopalakrishnan, W. K. Burns, and C. H. Bulmer, "Microwave-optical mixing in $LiNbO_3$ modulators," IEEE Trans. Microwave Theory Tech. **41**, 2383–2391 (1993).
20. G. K. Gopalakrishnan, R. P. Moeller, M. M. Howerton, W. K. Burns, K. J. Williams, and R. D. Esman, "A low-loss downconverting analog fiber-optic link," IEEE Trans. Microwave Theory Tech. **43**, 2318–2323 (1995).
21. Fiber-Span, application note, "Spurious free dynamic range," http://www.fiber-span.com/Application_Note_Spurious%20Free%20Dynamic%20Range.pdf.
22. Maxim Integrated, application note, "Three methods of noise figure measurement." http://www.maximintegrated.com/app-notes/index.mvp/id/2875.